Mass and Number Size Distributions of Refractory Black Carbon (rBC) in Snow and Firn Samples from Pine Island Glacier, West Antarctica

Luciano Marquetto[1,2], Susan Kaspari[1], Jefferson Cardia Simões[2,3]

[1] Department of Geological Sciences, Central Washington University, Ellensburg, Washington – USA. 98926.

[2] Centro Polar e Climático, Universidade Federal do Rio Grande do Sul, Av, Bento Gonçalves 9500, Porto Alegre, Rio Grande do Sul – Brazil. 91509-900.

[3] Climate Change Institute, University of Maine, Orono, Maine 04469-5790 – USA

Corresponding author: Luciano Marquetto (luciano.marquetto@gmail.com)

Key Points:

- First detailed rBC mass and number size distributions from snow and firn from West Antarctica
- rBC mass size distributions are bimodal with a primary mode at 160 nm and a secondary mode at 1880 nm
- Large particles (D_{BC} > 500 nm) are more common during the wet season than during the dry season

Abstract

An extended-range Single-Particle Soot Photometer (SP2) coupled to a Marin-5 nebulizer was used to measure the refractory black carbon (rBC) mass and number size distributions in 1004 samples from a West Antarctica snow/firn core. The SP2 was calibrated using Aquadag and a Centrifugal Particle Mass Analyzer for BC particles ranging from 0.5 to 800 fg. Our results from 1.03 x 10^6 particles indicate a significant contribution of rare, large particles of mass-equivalent diameter (D_{BC}) > 500 nm to the total rBC mass (36%), while small particles (D_{BC} < 100 nm) are abundant but contribute < 8% to total rBC mass. We observed a mass median diameter (MMD) of 160 nm, smaller than reported for snow comparing to other regions of the globe, but similar to East Antarctica rBC size distributions. In addition, we observed a secondary mode at 1880 nm, possibly originated from a combination of rBC aging processes in the atmosphere and particle agglomeration during snow formation/deposition. We compared two sets of samples from different seasons (wet vs. dry), and observed different contributions of large particles to the total rBC mass of each. Particles with D_{BC} > 500 nm contributed 45% and 33% of the total rBC mass for the wet and dry season, respectively, indicating that larger particles are more common during the wet season. Post-depositional processes (millimeter thick melt layers) have been observed in some samples, although they did not change the observed median diameter. This study provides the first detailed rBC size distribution from West Antarctica.

Plain Language Summary

Black carbon (BC) is a particle produced by the incomplete combustion of biomass burning and fossil fuels, and plays an important role in the climate system due to its strong light absorption properties. The size of BC particles in snow is important for determining the effects that BC has on the cryosphere, and provides insight into the processes controlling BC emission history, transport and deposition. Past studies indicate spatial differences of BC size distributions in snow, but these studies are limited in number, and more are needed to address this spatial variability. Here the size distribution is presented of BC particles from 1004 samples from a Pine Island Glacier ice core, West Antarctica, in a region where there is no information of BC particle size in snow. BC in West Antarctica is smaller than other regions of the globe, but large, rare particles are also present. These large BC particles are larger than what other studies have reported, and could be a result of long-range transport from other continents, and/or agglomeration from small particles during transport or deposition.

1 Introduction

Black carbon (BC) is a carbonaceous aerosol emitted by incomplete combustion of fossil fuels and biomass that affects the climate due to its strong light-absorption properties (Goldberg, 1985; IPCC, 2013). BC absorbs the most solar light per unit mass of any atmospheric aerosol (Schwarz et al., 2013), and when deposited on snow and ice, reduces albedo and accelerates melt (Bond et al., 2013; Hadley & Kirchstetter, 2012). Increases in BC concentrations since the industrial revolution have been observed in ice sheets and glaciers around the world (McConnell et al., 2007; Osmont, Wendl et al., 2018; Thevenon et al., 2009), with direct implications to the planetary albedo (Bice et al., 2009; Bond et al., 2013; Hansen & Nazarenko, 2004).

The impact of BC on snow albedo depends on a number of factors, including BC content in snow (He et al., 2018), mixtures with other particles (Warren & Wiscombe, 1980) and BC particle properties. BC size is the dominant source of uncertainty when estimating BC

absorption properties in snow (Schwarz et al., 2013). These authors state there is a possible overestimation of BC global mean snow forcing up to 30% as atmospheric BC size distributions, rather than snow BC size distributions, are used to model BC impacts in the cryosphere.

Previous studies have shown rBC size distribution in the atmosphere tend to follow a pure lognormal function, with a mass median diameter (MMD) of ~220 nm or smaller and less than 1% of total mass associated with particles of mass equivalent diameter (D_{BC}) > 600 nm (Schwarz et al., 2013). Urban atmosphere rBC MMD tends towards lower medians (~100 nm), while remote atmosphere rBC MMD present higher values (~220 nm - Schwarz et al., 2012, 2013), although the opposite has also been reported (Wu et al., 2017 and references therein).

The size distribution of rBC in snow presents a MMD similar to remote atmospheric sites (~220 nm - Lim et al., 2014; Schwarz et al., 2013), but deviates from a lognormal distribution due to the contribution of particles with D_{BC} > 500 nm. Schwarz et al. (2013) found that particles with D_{BC} > 600 nm represented 28% of the rBC mass in snow samples from rural and semi-rural Colorado, USA. This is an important observation, as BC absorption properties differs with particle size. When BC diameter is small relative to the light's wavelength, the particle absorbs light proportionally to its mass. However at larger sizes, light absorption is proportional to particle surface area (Schwarz et al., 2013).

In Antarctica, the literature about BC size distributions is still scarce, thus more observations are needed. The most extensive work was carried out by Kinase et al. (2019) for East Antarctica around Syowa Station. The authors found a bimodal distribution in BC in snow, with MMDs of ~140 nm and 690 nm and number median diameters (NMD) around 70 nm; post-depositional processes affected BC concentrations but not size distributions. Khan et al. (2018) presented rBC volume distributions (rather than MMD) showing large rBC particles of 300–400 nm in a shallow snow pit in McMurdo Dry Valleys. Ellis et al. (2016) observed a substantial fraction of small particles (D_{BC} < 90 nm) in East Antarctica snow and ice, although only qualitatively. Thus, further studies of Antarctic BC mass size distributions are necessary. Furthermore, as BC is mainly deposited in snow through wet deposition (Flanner et al., 2007), measuring the size distribution of BC particles in snow should improve our quantitative understanding of the BC wet removal mechanism from the atmosphere (Mori et al., 2016).

In this work we present the rBC number and mass size distributions of 1004 snow samples from a 20 meter snow/firn core (TT07) drilled in West Antarctica during the 2014/2015 austral summer, that spans 1968–2015 period (Marquetto et al., 2019, 2020). The rBC present in the core likely reflects long-range transport from sources in South America and Australia/New Zealand, and is associated mostly with biomass burning emissions (Arienzo et al., 2017; Bisiaux et al., 2012a; Koch et al., 2007; Stohl & Sodemann, 2010).

2 Site description and Field Campaign

The core presented in this study (TT07) was drilled on the Pine Island Glacier at 79°55'34.6"S, 94°21'13.3"W (elevation 2122 m a.s.l.), near the Mount Johns Nunatak (located 70 km NE of the drilling site) (Figure 1). The site was chosen due to (1) its relatively high accumulation rate (0.21 water equivalent meters per year); (2) being a drainage basin divide (between Pine Island and Institute glaciers); and (3) being an area where air masses from the Weddell, Amundsen and Bellingshausen seas converge (Schwanck et al. 2016).

The core was retrieved in twenty-one sections of less than 1 meter each, weighed in the field, packed in polyethylene bags and then stored in high-density Styrofoam boxes. It was sent by air to Punta Arenas (Chile), then to a deposit in Bangor (US) for storage and finally to the Central Washington University Ice Core Laboratory (Ellensburg, WA), where it was kept at -18°C in a clean cold room until sub-sampling and analysis. Borehole temperature measured in the field was -34°C at 12 meters deep. We used a probe previously calibrated that remained in the borehole for at least 8 hours.

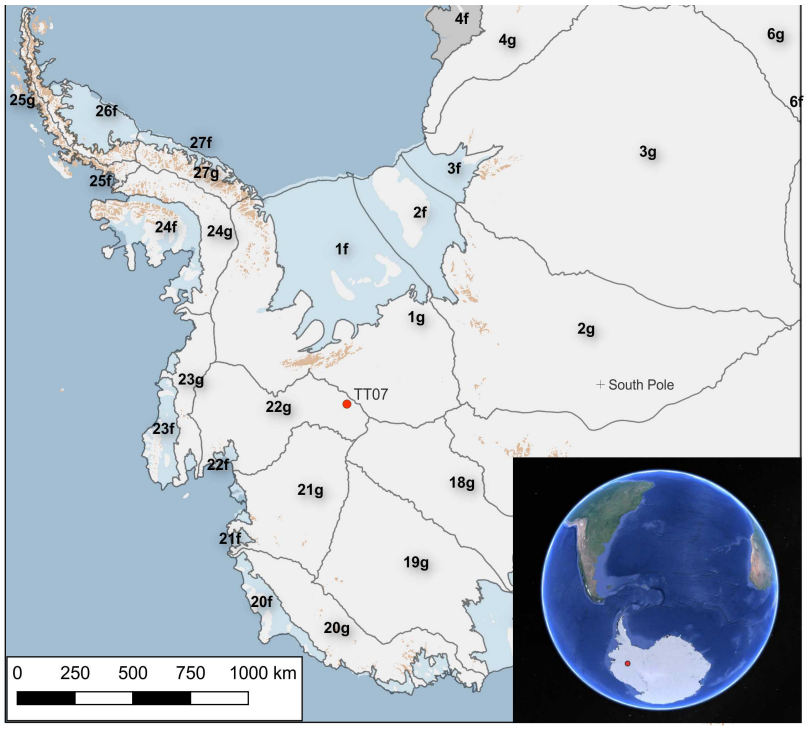

Figure 1. Drilling location for the snow/firn core analyzed in this work (TT07). Black lines show West Antarctic ice divides (1g = Institute Glacier; 22g = Pine Island Glacier). Data from BEDMAP 2 project (Fretwell et al., 2013). The bottom right shows the drilling site in perspective to South America.

3 Materials and Methods

3.1 General information on the SP2

We used an extended range Single Particle Soot Photometer (SP2) coupled to a Marin-5 nebulizer in the Department of Geological Sciences, Central Washington University (CWU), WA, USA to analyze the snow and firn samples. Data processing was performed with the SP2 Toolkit 4.200 developed by the Laboratory of Atmospheric Chemistry at Paul Scherer Institute (PSI), and was used on the scientific data analysis software IGOR Pro versions 6.3 and 7. Data is reported as refractory black carbon (rBC), following recommendations from Petzold et al. (2013).

The SP2 (Droplet Measurement Technologies - DMT, Boulder, CO, USA) is widely applied in aerosol science and is one of the most reliable instruments to analyze BC on a particle-by-particle basis (Wendl et al., 2014). It was adapted to analyze meltwater of snow and ice samples by McConnell et al. (2007), and since then it has been extensively used to analyze seasonal snow (*e.g.* Delaney et al., 2015; Schwarz et al., 2012), high-altitude glacier surface

snow and ice cores (*e.g.* Kaspari et al., 2011, 2014; Lim et al., 2017; Osmont et al., 2018; Sigl et al., 2018) and polar snow and ice (*e.g.* Arienzo et al., 2017; Bisiaux et al., 2012a, 2012b; Casey et al., 2017). The SP2 uses laser-induced incandescence to measure the rBC mass of individual particles as the peak intensity of light that a particle emits is proportional to its size and mass (Schwarz et al., 2006; Slowik et al., 2007). The SP2 rBC measurement is negligibly affected by other materials (Moteki & Kondo, 2010; Schwarz et al., 2006, 2012).

These characteristics allow the SP2 to reconstruct accumulation-mode size distributions of rBC from samples (Schwarz et al., 2010), as the indirect mass measurement can be then converted to size using the equation:

Eq. 1

$$D_{BC} = \left(\frac{6\,M}{\pi\,\rho_{true}}\right)^{1/3}$$

where D_{BC} is the rBC particle mass equivalent diameter, M is the particle mass and ρ_{true} is the true density of the particle considered (commonly assumed to be 1800 kg m^{-3} or 1.8 g cm^{-3}; Moteki & Kondo, 2010). Mass equivalent diameter is also presented in the literature as D_{MEV} (Cheng et al., 2018).

The standard SP2 detects particles in the 70–500 nm mass-equivalent diameter (D_{BC}) range (DMT, 2013b), but CWU has an extended-range SP2, capable of detecting particles between 80–2000 nm D_{BC} (assuming a black carbon density of 1.8 g cm^{-3}). For details of the extended range SP2, see Mori et al. (2016) and Moteki and Kondo (2010).

3.2 Sample preparation

Details on laboratory and cold room cleaning, as well as the cut plan for the samples is presented in Marquetto et al. (2020). Briefly, the samples were hand scraped with a clean ceramic knife in a laminar flow hood inside a cold room, to remove the outer snow/firn layer (2–4 mm). They were stored in pre-cleaned 50-mL polypropylene vials and kept frozen until analysis. Just prior to analysis, the samples were melted at room temperature or in a warm bath and sonicated for 15 minutes prior to analysis. Most samples were analyzed in less than 30 minutes after melting, and all samples were analyzed in less than two hours after melting.

3.3 Sample nebulization

As the SP2 was initially designed to analyze BC from the atmosphere (dry aerosol), it is necessary to nebulize the sample before it enters the SP2 inlet. For this step, we used a CETAC Marin-5 nebulizer.

The nebulization step induces losses of rBC particles during the sample analysis (imperfect nebulization, removal of rBC with the drain water, adsorption of rBC at the surface of the capillaries), meaning that only a fraction of BC particles initially pumped from the sample will reach the SP2 inlet (Katich et al., 2017). This fraction corresponds to the nebulization efficiency. Previous works have shown that the Marin-5 nebulization efficiency is not size dependent in the 200–3000 nm diameter range (Katich et al., 2017; Mori et al., 2016).

In this work we assume that the melting and nebulization processes do not cause BC agglomeration that would shift the size distribution to larger sizes, based on the same

assumptions as Schwarz et al. (2013). Thus, we consider the mass size distribution curve obtained by the SP2 to represent the original rBC size distribution of the snow samples.

3.4 SP2 calibration

The SP2 needs empirical calibration to assign a BC mass to a given SP2 response, referred to as internal calibration by Wendl et al. (2014). The internal calibration is obtained by recording the average incandescent signal peak height for pure BC particles of a known mass over the whole dynamic range of the SP2 (Gysel et al., 2011). An additional calibration, called external calibration, is necessary when analyzing liquid samples to correct for BC losses during the nebulization process.

The internal calibration was carried out on CWU's SP2 using a Centrifugal Particle Mass Analyzer (CPMA) to mass-select BC particles of a known polydisperse BC standard consisting of Aquadag (Acheson Industries Inc., Port Huron, MI, USA) diluted in Milli-Q water (MilliQ-Element, Millipore, Milford, USA; 18,2 M Ω). Aquadag was also used for the daily SP2 external calibration (details of the external calibration are in Marquetto et al., 2020).

The use of a CPMA to mass-select BC particles in the SP2 internal calibration is recommended in Schwarz et al. (2012) to reduce uncertainties associated with detection of large rBC particles. Particle mass analyzers select particles by their mass-to-charge ratio by balancing electrostatic and centrifugal forces, and are a better choice for particle calibration than Differential Mobility Analyzers (DMA) as the latter classifies particles by size and thus needs further corrections along with BC density assumptions in order to calculate the particle mass (Gysel et al., 2011; Olfert & Collings, 2005). Also, the CPMA has an uncertainty of only 1.4% in mass measurements for single-charge particle (Symonds et al., 2013).

We configured the CPMA to select 23 particle masses from 0.5 fg to 800 fg (translating to D_{BC} ~ 80 – 1000 nm); each mass was measured for 30 min to 6 hours to provide statistically significant particle triggers to calibrate the SP2. Most literature about BC in snow and ice used a DMA for calibration, and ran up to particle sizes equivalent to 100 fg (Katich et al., 2017; Lim et al., 2014; Osmont et al., 2018; Schwarz et al., 2012); some extended further (Lim et al., 2017 - 220 fg; Mori et al., 2016 - 300 fg). Moteki and Kondo (2010) extended their calibration up to 400 fg with Aquadag and to 800 fg with Glassy Carbon (although the later consists of >400 nm spherical, compact particles, different from ambient soot). To our knowledge, no calibration as broad as this work (0.5–800 fg) using a CPMA is documented in the literature.

The use of Aquadag for the SP2 internal and external calibrations is described in the literature (Gysel et al., 2011; Nobuhiro Moteki & Kondo, 2010) and recommended because the SP2 sensitivity to its BC-type is known, and its mass-size distribution most closely represents the mass size distributions observed in snow: ~100–1000 nm (Wendl et al., 2014). Also, regarding particle morphology, Aquadag is characterized by fluffy aggregates of thin flakes and small spherules of crystalline graphite (Moteki et al., 2009), similar to non-compact ambient soot (Moteki & Kondo, 2010).

Extrapolations of the calibration limits (80–1000 nm) to the full detection limits of the CWU SP2 (80–2000 nm) were made based on the relationship between particle mass and incandescent signal. Moteki & Kondo (2010) observed that for small particles (M < 10 fg) the incandescent signal is linearly proportional to particle mass, while the relationship for larger

particles (10 fg < M < 800 fg) is dependent on particle shape and calculated using an empirical power-law:

Eq. 2

$$P_h = AM^b$$

Where P_h is the incandescent peak height measured by the SP2, A is a fitted variable, M is the rBC particle mass and b is a variable anti-correlated to the material's density (Moteki & Kondo, 2010; Schwarz et al., 2012). The parameter b increases (up to the Rayleigh-Gans approximation of 1) for particles of non-compact shapes and approaches 2/3 (=0.667) for particles of extremely compact shapes (Moteki & Kondo, 2010). These observations, though, were made using a DMA for the SP2 internal calibration. In the internal calibration carried out in this work we observed that the polynomial splines (least squares fit) from the PSI SP2 toolkit presented the best fit both in the lower and higher end of the SP2 detection range, so we used these for extrapolation. When necessary to adjust the curvature of the calibration curve at the low end, the fits were adjusted by segments as described in DMT (2013a). The power law and the linear fit from Moteki and Kondo (2010) do not agree with our calibration data as well as the polynomial splines in the lower and higher end of the calibrated ranges (Figures 2a–c).

The data presented in this work was obtained from the duplicated extended range broadband detector of the SP2 (the combination of the high gain and low gain amplifications: B2HG+B2LG). These channels presented the best fit calibration curve of all channels, with a precise fitting in the lower (B2HG) and higher (B2LG) end of the particle mass range (calibration curves in Figure 2). The B2HG channel was able to detect particles in the 80–600 nm size range, while the B2LG detection range was 80–2000 nm. As expected from previous works (Mori et al., 2016; Moteki & Kondo, 2010), the incandescence peak height observed in the internal calibration for larger particles is not linearly correlated to their mass as particle effective density (ρ_{eff}) is $\neq 0$. ρ_{eff} is a measure of the compactness of the particle shape, and can vary from zero for extremely non-compact particles (highly branched aggregates), up to the true density ($\sim$1.8 g cm^{-3}) for extremely compact particles (spherical) (Moteki & Kondo, 2010).

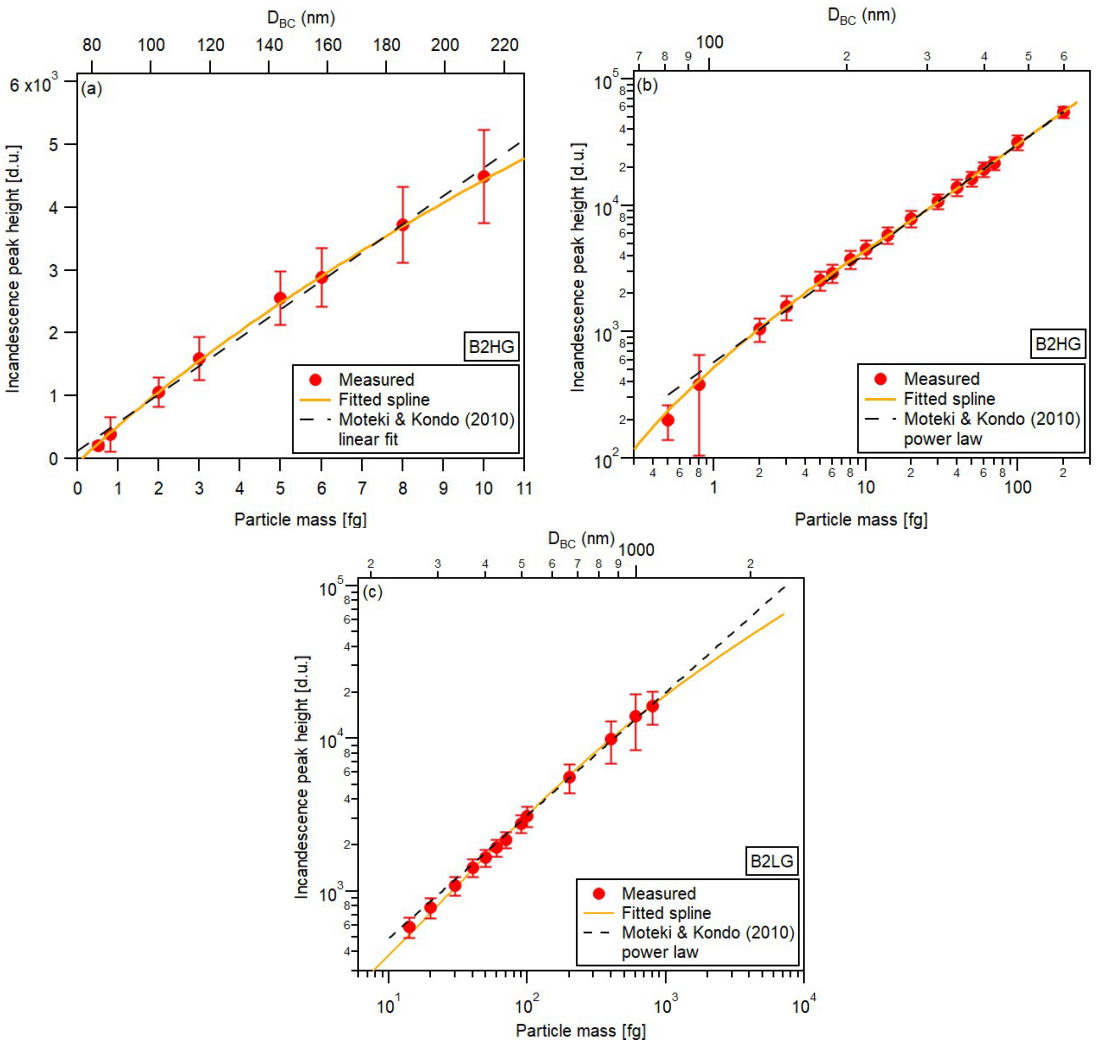

Figure 2. Calibration curves for the (a) B2HG channel (0.5 < M < 10 fg – linear scale), (b) B2HG channel (0.5 < M < 200 fg – logarithmic scale) and (c) B2LG channel (14 < M < 800 fg – logarithmic scale), obtained from the internal calibration carried out using the SP2+CPMA. The B2HG channel showed a good fit for low mass particles (0.5–200 fg), while the B2LG channel presented a good fit for larger particles (200–800 fg). Also shown for comparison are the measured relationships from Moteki & Kondo (2010) – linear fit for M < 10 fg and power law for 20 < M < 800 fg. Incandescence peak height is presented in (arbitrary) defined units (d.u.). Particle size was calculated using the formula presented in section 3.1, assuming ρ_{true} as 1.8 g cm $^{-3}$. Error bars represent one standard deviation of mean peak height (Table 1 in the supplement present more results of calibration time, particle triggers and mean peak height ± standard deviation for each calibration mass).

3.5 Sample concatenation and seasonal classification

To achieve a statistically significant rBC size distribution it is necessary to collect a large number of rBC particles in the SP2. Katich et al. (2017) empirically determined this number to be ~40,000 particles for typical ambient snow, although this number could be much higher if rare, large rBC particles are present in the sample, as these could change the size distribution towards larger values.

Considering the low BC concentration in the samples, especially in the wet season (as low as 200 particles / sample), we present our results as a concatenation of individual samples in

seasonally resolved samples (dry season = summer/fall; wet season = winter/spring). Although the concatenated dry season presented considerably more particles ($n = 8.28 \times 10^5$) than the wet season ($n = 2.03 \times 10^5$), both sets have a robust number of collected particles.

Seasonal sample discrimination was based on the core dating presented in Marquetto et al. (2020). Antarctic ice core BC records show a well-defined seasonality, with peak concentrations in the dry season due to increased biomass burning activity in the Southern Hemisphere (SH) during this time of the year (Bisiaux et al., 2012b; Sand et al., 2017; Winstrup et al., 2017); the wet season is identified by much lower BC concentrations. The core presented in this study was dated to 47 years and showed geometrical mean concentration of 0.06 μg L^{-1} for the dry season and 0.01 μg L^{-1} in the wet season (Marquetto et al., 2020). As for BC size distribution, we considered only results in the CWU SP2 calibration range (80 nm > D_{BC} > 2000 nm).

4 Results and discussion

4.1 Size distribution of rBC in the Antarctic snow samples

Figure 5 shows the mass and number size distributions for the full set of samples. We observed the mass size distribution presented a primary mode, corresponding to particles of 160 nm, as well as a secondary mode at 1880 nm, near the upper detection limit.

The number counting of BC particles (N_{BC}) indicates most particles analyzed are of very small size. Particles with D_{BC} < 100 nm were abundant (45% of the total N_{BC} between 80 and 2000 nm), but represent only 7.4% of the total mass. Particles with D_{BC} > 500 nm, on the other hand, proved to be very rare (0.46% of the total N_{BC} between 80 and 2000 nm), but represent 36.4% of the total rBC mass. These results indicate that large particles exist in Antarctic snow and ice, and that despite their low occurrence, these particles can represent an important fraction of total rBC mass in the snow.

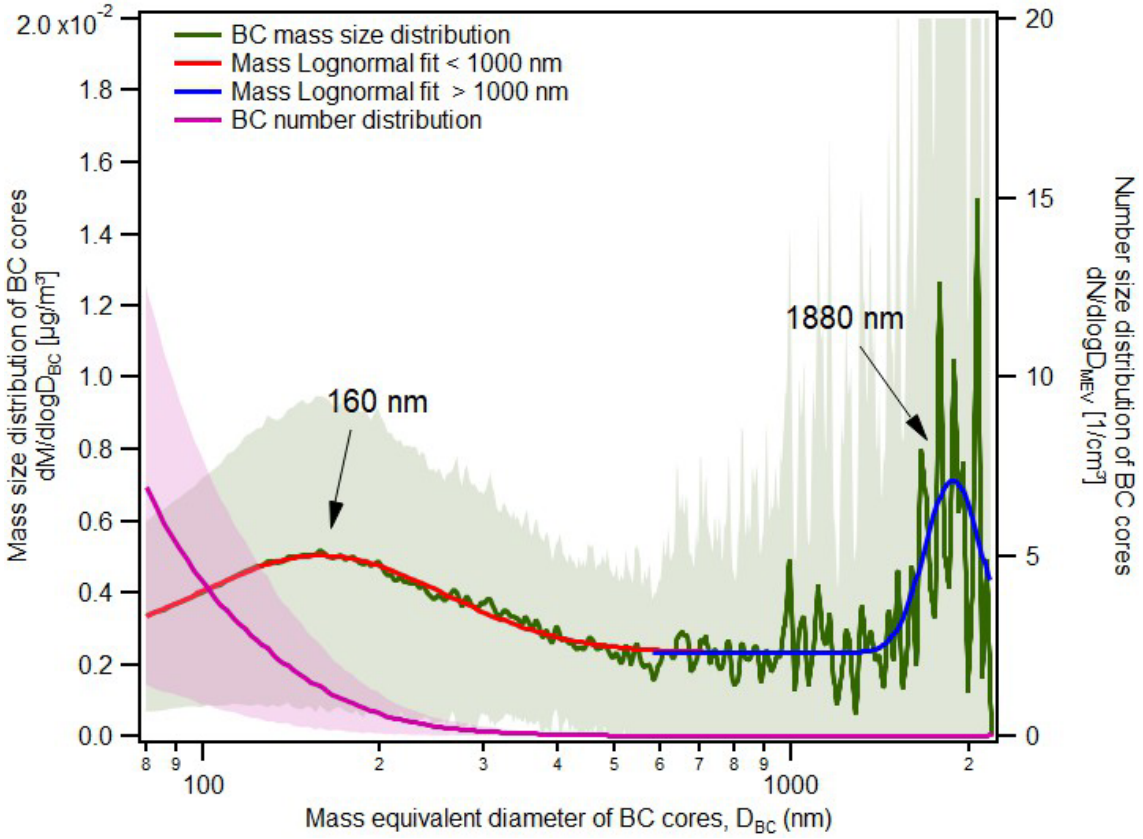

Figure 3. Mass and number size distributions for the full set of samples. Shaded areas represent one standard deviation (68.3%) of the number distribution (shaded purple) and mass distribution (shaded gray). Arrows indicate the two modes observed in the Antarctic samples mass distribution. Standard deviation for D_{BC} > 1500 nm (up to 2.5 times the scale) not shown.

As for seasonal variations (Figure 6, Table 1), particles with D_{BC} < 100 nm represent ~48% of all rBC N_{BC} both in the dry and wet season, and 8.5% (dry season) and 6.7% (wet season) of total rBC mass. The mass size distribution for both seasons is also similar to the full core, with the MMD at 160 nm. We observed, though, that the contribution of particles with D_{BC} > 500 nm to total rBC mass is higher in the wet season than in the dry season: 45.4% against 33.3%, and represent 0.38% and 0.21% of all rBC particles in each season, respectively. The seasonal differences may indicate different rBC origins, transport, aging or deposition processes for both seasons.

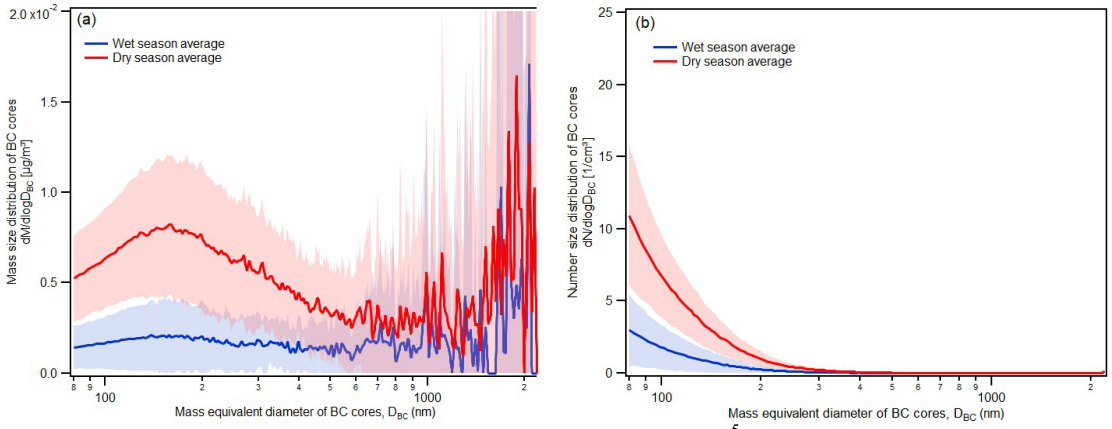

Figure 4. Mass and number size distributions for the dry (n = 8.28 x 10^5 particles) and wet season (n = 2.03 x 10^5 particles). Shaded areas represent one standard deviation (68.3%) of the wet (shaded blue) and dry (shaded red) seasons. Standard deviation for D_{BC} > 1500 nm (up to 2.5 times the scale) not shown in 6a.

Table 1. Comparison between the full core, dry season and wet season number and mass size distributions.

	Full core	Dry season	Wet season
MMD	160 nm	160 nm	160 nm
NMD	< 80 nm	< 80 nm	< 80 nm
D_{BC} < 100 nm mass	7.4%	8.5%	6.7%
D_{BC} < 100 nm number	45.4%	47.9%	48.0%
D_{BC} > 500 nm mass	36.4%	33.3%	45.4%
D_{BC} > 500 nm number	0.25%	0.21%	0.38%

We observed millimeter thick ice layers in the core's stratigraphy, likely associated with summer melting due to solar radiation in austral summer. However, these samples are not necessarily associated with high BC concentrations, as they ranged from as low as 0.02 to 0.08 µg L^{-1}. Also, they did not present MMD differences compared to samples of similar concentrations but with no ice layers (not shown). This suggests the melting was not an important post-depositional process for rBC. This result is supported by Doherty et al. (2013) that found only very limited redistribution of BC in a snow and firn vertical profile with melt layers much thicker (>10cm) than the ones found in TT07 (~1mm).

4.2 Comparison with other studies

Figure 7a compares the rBC mass distribution observed in the Antarctic samples with previous studies in snow from different parts of the globe, and Table 2 summarizes them. Ohata et al. (2013) analyzed 20 snow samples from Sapporo, a semi urban area in northern Japan; Schwarz et al. (2013) analyzed five fallen snow samples from three snowfalls in semi-rural and

322 rural areas of Denver, CO, USA; Sinha et al. (2018) analyzed 167 samples of different types
323 (fresh snow, falling snow and from the snowpack) from Ny-Ålesund, Spitsbergen; Mori et al.
324 (2019) did an extensive work analyzing the size distribution of BC in 296 samples from the
325 snowpack over Finland, Alaska, Siberia, Greenland and Spitsbergen during early spring in 2012–
326 2016. At last, for Antarctica, Kinase et al. (2019) analyzed the mass and size distribution of 58
327 snow samples collected from April to December 2011 at Syowa station (East Antarctica) and
328 along a traverse route to an inland (Mizuho) station, and Khan et al. (2018) presented an
329 averaged rBC volume distribution of 11 samples from a snow pit in the McMurdo Dry Valleys,
330 West Antarctica. We do not include results from Khan et al. (2018) as rBC volume distribution
331 differs from size distributions presented here.

332 The MMD of the samples analyzed in this work is similar to Kinase et al. (2019) for East
333 Antarctica, and smaller than the MMDs observed for snow in other regions of the globe.. As for
334 the number distribution, the Antarctic samples from this study presented a slightly lower but still
335 similar NMD than other very remote regions (East Antarctic samples from Kinase et al., 2019)
336 and Greenland samples from Mori et al. (2019), while differing greatly from more populated
337 areas (Sapporo samples from Ohata et al., 2013) and Ny-Ålesund samples from Sinha et al.
338 (2018).

339 While other studies have shown the contribution of particles with D_{BC} > 500 nm to total
340 mass in snow (*e.g.* for the USA (Schwarz et al., 2013); Spitzbergen (Sinha et al., 2018); the
341 Arctic (Mori et al., 2019); East Antarctica (Kinase et al., (2019)), and in the (Chinese)
342 atmosphere (Huang et al. (2011); Wang et al. (2014) and Wu et al. (2017)), our results showed
343 the highest contribution of all (Figure 7; Table 2). The snow samples from Japan (Ohata et al.,
344 2013), USA (Schwarz et al., 2013), and Spitzbergen (Sinha et al., 2018), do not present a
345 secondary mode, although particles with D_{BC} > 500 nm represent ~25% of the total mass in
346 Spitzbergen (Sinha et al., 2018) and ~30% in the USA (Schwarz et al., 2013). The samples from
347 East Antarctica (Kinase et al., 2019) show a secondary mode at ~690 nm and some of the Arctic
348 samples (Mori et al., 2019) presented secondary modes around 1200–1400 nm, closer to the
349 1880 nm found in this work.

350

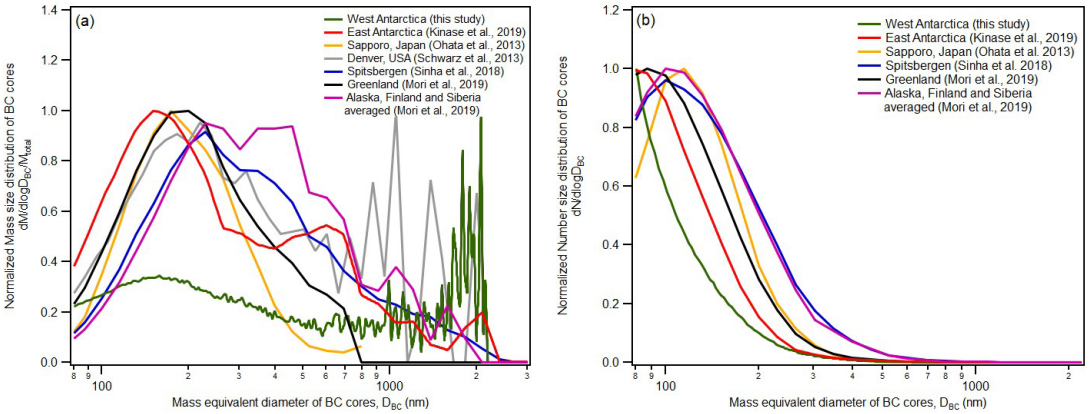

Figure 5. (a) Mass size distribution and **(b)** number distribution in snow from this work in comparison to previous studies in snow. Data was normalized so maximum values equals 1. Data from Alaska, Finland and Siberia (Mori et al., 2019) were averaged together to maintain figure readability (results were similar to each other).

Table 2. Size distribution in snow (MMD and NMD) from different parts of the globe and related references.

Location	Reference	Number of samples	Type of sample	MMD (nm)	Secondary MMD (nm)	NMD (nm)
West Antarctica	This work	1004	Snow/firn core	160	1880	< 80
West Antarctica	Khan et al. (2018)	11	Snowpit	300–400	-	-
East Antarctica	Kinase et al. (2019)	58	Surface snow	140	690	< 80
Sapporo, Japan	Ohata et al. (2013)	20	Surface snow	175	-	115
Denver, USA	Schwarz et al. (2013)	5	Surface snow	220	-	-
Ny-Ålesund, Spitsbergen	Sinha et al. (2018)	167	Fresh snow, falling snow and snowpack	240	-	102
Finland	Mori et al. (2019)	11	Snowpack and surface snow	358	-	110
Greenland	Mori et al. (2019)	68	Snowpack and surface snow	200	-	90
Alaska	Mori et al. (2019)	182	Snowpack and surface snow	320	1200–1400	100
Siberia	Mori et al. (2019)	29	Snowpack and surface snow	300	-	105

358

359 4.3 Size distribution interpretation

360 The rBC size distribution in snow can be affected by several factors: emission type
361 (biomass or fossil fuel burning), aging, transport, removal from the atmosphere and post-
362 depositional processes (Bond et al., 2013).

363 The formation of rBC particles is a complex process that depends on oxygen/fuel mixing
364 states and involves a series of reactions of polycyclic aromatic hydrocarbon molecules. Different
365 burning origins (*e.g.* open biomass burning, fossil fuel combustion) generate different particle
366 morphologies, size distributions and MMDs (Bond et al., 2013). Even the same burning origin
367 generates BC with different characteristics as the process evolves, as happens when biomass
368 burning changes from flaming to smoldering (Reid et al., 2005).

369 Aging in the atmosphere, agglomeration of water-bound rBC particles and size selection
370 during snow formation and deposition would also influence BC size distribution in snow
371 (Schwarz et al., 2013). Post-depositional processes also influence BC distributions (Doherty et
372 al., 2013), although this happens due to snow melt, which was very limited in the sampling site
373 (~1 mm each melt layer). Other post-depositional processes such as agglomeration of BC via
374 impaction of snowflakes or wind remobilization are unlikely without the presence of melt, due to
375 the extreme volume dilution of BC in the snow (Schwarz et al., 2013).

376 The NMD observed in the Antarctic samples in this work (< 80 nm) is similar to the
377 NMD observed in Greenland snow (~90 nm - Mori et al., 2019) and in East Antarctica (~70 nm -
378 Kinase et al., 2019). This is also in agreement to previous qualitative observations that found
379 abundant small rBC spherules with D_{BC} ~ 30 nm in Antarctic snow and ice (Ellis et al., 2016). A
380 NMD in the Aitken mode (less than 100 nm diameter) is commonly related to fresh, high
381 temperature BC emissions, originated from efficient fuel burning (Bond et al., 2013), although
382 we consider unlikely that this NMD is related to fossil-fuel combustion. The sampling site is a
383 remote place, with no nearby anthropogenic activity. Also, previous works (Arienzo et al., 2017;
384 Bisiaux et al., 2012a; Koch et al., 2007; Stohl & Sodemann, 2010) stated that BC in Antarctica
385 mostly reflects long-range transport of biomass burning emissions from South America and
386 Australia. At last, Ellis et al. (2016) observed these small BC spherules with D_{BC} ~ 30 nm in
387 Antarctic ice dated to year 1759 C.E. (before industrialization), which cannot reflect fossil fuel
388 emissions. They did not observe discernable differences in BC morphology and sizes between
389 the different time periods studied (pre and post industrialization), which also corroborates the
390 biomass burning likely origin.

391 Pan et al. (2017) state that flaming combustion tends to produce larger rBC particles
392 (MMD ~215 nm) than smoldering combustion (MMD ~152 nm) due to less efficient transport of
393 oxygen into the interior flame zone and consequent increase in coagulation rates. The smaller
394 MMD found in this work could thus reflect a significant contribution of smoldering to BC
395 emissions reaching Antarctica, even though most rBC particles are emitted during the flaming
396 stage (Reid et al., 2005).

397 As for the larger particles, aging processes tend to increase BC particle size (Bond et al.,
398 2013), which could explain some of the contribution of particles with D_{BC} > 500 nm to the total
399 rBC in the samples. Size dependent removal (Moteki et al., 2012) and coagulation processes
400 dominated by Brownian motion (Wang et al., 2015) have been suggested to increase BC size.

Although these processes have been observed in the ambient, the former do not increase significantly the mass of rBC with D_{BC} > 500 nm (Schwarz et al., 2013) and the latter is too slow to increase rBC particles to D_{BC} > 500 nm in the aerosol average lifetime (7-10 days) (Huang & Yu, 2008). Instead, in-cloud processes involving addition of sulfate seems to be a cause of significant growth for rBC particles with D_{BC} > 500 nm (Huang & Yu, 2008). Long-range transport of these large particles generated in the atmosphere far away from Antarctica have been suggested by Ellis et al. (2016), which is not unreasonable considering mineral dust up to 5000 nm can be transported over long distances (Gaiero et al., 2007; Mahowald et al., 2014) and be deposited in Antarctic snow (Delmonte et al., 2013; Li et al., 2008). Dust up to 2400 nm has been found at the sampling site, associated with remote continental sources (*e.g.* South America - Cataldo et al., 2013; Schwanck et al., 2017), suggesting that large BC particles could also be transported this far.

Nonetheless, larger BC particles have more condensation nuclei activity than smaller ones (Dusek et al., 2006), which means the former would be removed more easily from the atmosphere than the latter and thus the final BC size distribution would decrease with distance. In addition to that, Schwarz et al. (2013) reported a significant contribution of large rBC particles to the size distribution of semi-rural and rural snow near Denver, CO (USA) that underwent only limited aging. This suggests that aging processes in the atmosphere cannot fully explain the contribution of large rBC particles to total rBC mass. Based on Dusek et al. (2006) and Schwarz et al. (2013), we hypothesize that processes acting during snow formation in the atmosphere and during snow deposition have a significant role in rBC size in snow. Unfortunately, we do not have BC measurements of the atmosphere at the drilling site to compare both size distributions to test this hypothesis. Further studies on this topic would be of extreme value to improve our understanding in BC deposition in snow.

5 Conclusions

Measurements of rBC size distributions in snow are important to adequately model BC impacts on the cryosphere, but are still scarce. In this work we presented a rBC size distribution obtained from a 20 meters-deep snow/firn core from West Antarctica (1004 melted samples). Results show an MMD of 160 nm, that we attributed to biomass burning (smoldering), although this MMD is smaller than commonly observed from biomass burning origin. A secondary mode was observed at 1880 nm, which we attributed, based on the literature, to a combination of factors: emission type (uncontrolled biomass burning), aging processes (in-cloud processes involving addition of sulfate to the rBC particle) and agglomeration of water-bound rBC particles during snow formation/deposition in the site. Our results are similar to recently published literature about East Antarctica rBC size distributions (Kinase et al., 2019), that found a primary MMD of ~140 nm, although the secondary mode observed in this study is bigger than the one observed in Kinase et al. (2019) (~1880 nm against ~690 nm, respectively). We consider post-depositional processes to have negligible influence to rBC size distribution due to very limited melt and to the extreme volume dilution of BC in the snow. Small particles (80 nm < D_{BC} < 100 nm) are abundant, accounting for 45.4% of all rBC cores detected by the SP2, but do not add significantly to rBC total mass (7.4%). Large particles (500 nm > D_{BC} > 2000 nm) are very rare (0.25%) but represent a large portion of rBC total mass (36.4%). Contribution of particles with D_{BC} > 500 nm were higher in the wet season (mass: 45.4%, number: 0.38%) than in the dry season (mass: 33.3%, number: 0.21%), but no other seasonal difference was observed in the distributions. These results corroborate the findings by Schwarz et al. (2013) that snow size

446 distribution present a significant contribution of larger particles to total rBC mass, much larger
447 than atmospheric rBC size distributions. Also, our results indicate that large particles exist in
448 Antarctic snow and ice, and that despite their low occurrence, they can represent an important
449 fraction of total rBC mass in the snow. More research comparing rBC size distributions in snow
450 and in the air above it would be of great value to improve the understanding of rBC deposition in
451 snow and the role of aging and snow formation processes to size distributions.

452 **Acknowledgments, Samples, and Data**

453 This research is part of the Brazilian Antarctic Program (PROANTAR) and was financed
454 with funds from the Brazilian National Council for Scientific and Technological Development
455 (CNPq) Split Fellowship Program (no. 200386/2018-2), from the CNPq projects 465680/2014-3
456 and 442761/2018-0, CAPES project 'INCT da Criosfera' 88887.136384/2017-00 and
457 PROANTAR project 88887.314450/2019-00. We thank the Centro Polar e Climático
458 (CPC/UFRGS) and the Department of Geological Sciences (CWU) faculty and staff for
459 supporting this work. We also thank authors of Khan et al. (2018), Kinase et al. (2019), Ohata et
460 al. (2013), Schwarz et al. (2013), Sinha et al. (2018) and Mori et al. (2019) for data availability.
461 The authors declare no conflict of interests of any kind. rBC size distribution data is presented as
462 a supplement of this manuscript, for the review process, and will be made available in an online
463 repository after manuscript acceptance.

464 **References**

465 Arienzo, M. M., McConnell, J. R., Murphy, L. N., Chellman, N., Das, S., Kipfstuhl, S.,
466 Mulvaney, R. (2017). Holocene black carbon in Antarctica paralleled Southern Hemisphere
467 climate. *Journal of Geophysical Research*, *122*(13), 6713–6728.
468 https://doi.org/10.1002/2017JD026599

469 Bice, K. L., Eil, A. G., Habib, B., Heijmans, P. L., Kopp, R., Nogues, J., Norcross, F. Sweitzer-
470 Hamilton, M., Whitworth, A.. (2009). *Black carbon: A review and policy recommendations*.
471 *Woodrow Wilson School of public and international affairs*. Princeton, NJ, EUA. Retrieved
472 from
473 http://scholar.google.com/scholar?hl=en&btnG=Search&q=intitle:Black+Carbon:+A+Revie
474 w+and+Policy+recommendations#0

475 Bisiaux, M. M., Edwards, R., McConnell, J. R., Curran, M. A. J., Van Ommen, T. D., Smith, A.
476 M., Meumann, T. A., Pasteris, D. R., Penner, J. E., Taylor, K. (2012). Changes in black
477 carbon deposition to Antarctica from two high-resolution ice core records, 1850-2000 AD.
478 *Atmospheric Chemistry and Physics*, *12*(9), 4107–4115. https://doi.org/10.5194/acp-12-
479 4107-2012

480 Bisiaux, M. M., Edwards, R., McConnell, J. R., Albert, M. R., Anschütz, H., Neumann, T.,
481 Isaksson, E., Penner, J. E. (2012). Variability of black carbon deposition to the East
482 Antarctic Plateau, 1800-2000 AD. *Atmospheric Chemistry and Physics*, *12*(8), 3799–3808.
483 https://doi.org/10.5194/acp-12-3799-2012

484 Bond, T. C., Doherty, S. J., Fahey, D. W., Forster, P. M., Berntsen, T., Deangelo, B. J. et al.
485 (2013). Bounding the role of black carbon in the climate system: A scientific assessment.

Journal of Geophysical Research: Atmospheres, *118*(11), 5380–5552. https://doi.org/10.1002/jgrd.50171

Casey, K. A., Kaspari, S. D., Skiles, S. M., Kreutz, K., Handley, M. J. (2017). The spectral and chemical measurement of pollutants on snow near South Pole, Antarctica. *Journal of Geophysical Research: Atmospheres*, *122*(12), 6592–6610. https://doi.org/10.1002/2016JD026418

Cataldo, M., Evangelista, H., Simões, J. C., Godoi, R. H. M., Simmonds, I., Hollanda, M. H., Wainer, I. Aquino, F. (2013). Mineral dust variability in central West Antarctica associated with ozone depletion. *Atmospheric Chemistry and Physics*, *13*(4), 2165–2175. https://doi.org/10.5194/acp-13-2165-2013

Cheng, Y., Li, S. M., Gordon, M., Liu, P. (2018). Size distribution and coating thickness of black carbon from the Canadian oil sands operations. *Atmospheric Chemistry and Physics*, *18*(4), 2653–2667. https://doi.org/10.5194/acp-18-2653-2018

Delaney, I., Kaspari, S., Jenkins, M. (2015). Black carbon concentrations in snow at Tronsen Meadow in Central Washington from 2012 to 2013: Temporal and spatial variations and the role of local forest fire activity. *Journal of Geophysical Research: Atmospheres*, *120*, 9160–9172. https://doi.org/10.1002/2017JD027560

Delmonte, B., Baroni, C., Andersson, P. S., Narcisi, B., Salvatore, M. C., Petit, J. R., Scarchilli, C., Frezzotti, M., Albani, S, Maggi, V. (2013). Modern and Holocene aeolian dust variability from Talos Dome (Northern Victoria Land) to the interior of the Antarctic ice sheet. *Quaternary Science Reviews*, *64*, 76–89. https://doi.org/10.1016/j.quascirev.2012.11.033

Doherty, S. J., Grenfell, T. C., Forsström, S., Hegg, D. L., Brandt, R. E., Warren, S. G. (2013). Observed vertical redistribution of black carbon and other insoluble light-absorbing particles in melting snow. *Journal of Geophysical Research: Atmospheres*, *118*(11), 5553–5569. https://doi.org/10.1002/jgrd.50235

Dusek, U., Frank, G. P., Hildebrandt, L., Curtius, J., Schneider, J., Walter, S. et al. (2006). Size matters more than chemistry for cloud-nucleating ability of aerosol particles. *Science*, *312*(5778), 1375–1378. https://doi.org/10.1126/science.1125261

Ellis, A., Edwards, R., Saunders, M., Chakrabarty, R. K., Subramanian, R., Timms, N. E. et al. (2016). Individual particle morphology, coatings, and impurities of black carbon aerosols in Antarctic ice and tropical rainfall. *Geophysical Research Letters*, *43*(22), 11,875-11,883. https://doi.org/10.1002/2016GL071042

Flanner, M. G., Zender, C. S., Randerson, J. T., Rasch, P. J. (2007). Present-day climate forcing and response from black carbon in snow. *Journal of Geophysical Research Atmospheres*, *112*(11), 1–17. https://doi.org/10.1029/2006JD008003

Fretwell, P., Pritchard, H. D., Vaughan, D. G., Bamber, J. L., Barrand, N. E., Bell, R. et al. (2013). Bedmap2: Improved ice bed, surface and thickness datasets for Antarctica.

Cryosphere, *7*(1), 375–393. https://doi.org/10.5194/tc-7-375-2013

Gaiero, D. M., Brunet, F., Probst, J. L., Depetris, P. J. (2007). A uniform isotopic and chemical signature of dust exported from Patagonia: Rock sources and occurrence in southern environments. *Chemical Geology*, *238*(1–2), 107–120. https://doi.org/10.1016/j.chemgeo.2006.11.003

Goldberg, E. D. (1985). *Black Carbon in the Environment* (1st ed.). New York: Wiley.

Gysel, M., Laborde, M., Olfert, J. S., Subramanian, R., Gréhn, A. J. (2011). Effective density of Aquadag and fullerene soot black carbon reference materials used for SP2 calibration. *Atmospheric Measurement Techniques*, *4*(12), 2851–2858. https://doi.org/10.5194/amt-4-2851-2011

Hadley, O. L. & Kirchstetter, T. W. (2012). Black-carbon reduction of snow albedo. *Nature Climate Change*, *2*(6), 437–440. https://doi.org/10.1038/nclimate1433

Hansen, J. & Nazarenko, L. (2004). Soot climate forcing via snow and ice albedos. *Proceedings of the National Academy of Sciences of the United States of America*, *101*(2), 423–428. https://doi.org/10.1073/pnas.2237157100

He, C., Liou, K. N., Takano, Y. (2018). Resolving Size Distribution of Black Carbon Internally Mixed With Snow: Impact on Snow Optical Properties and Albedo. *Geophysical Research Letters*, *45*(6), 2697–2705. https://doi.org/10.1002/2018GL077062

Huang, X.-F. & Yu, J. Z. (2008). Size distributions of elemental carbon in the atmosphere of a coastal urban area in South China: characteristics, evolution processes, and implications for the mixing state. *Atmospheric Chemistry and Physics*, *8*(19), 5843–5853. https://doi.org/10.5194/acp-8-5843-2008

Huang, X. F., Gao, R. S., Schwarz, J. P., He, L. Y., Fahey, D. W., Watts, L. A. et al. (2011). Black carbon measurements in the Pearl River Delta region of China. *Journal of Geophysical Research Atmospheres*, *116*(12). https://doi.org/10.1029/2010JD014933

IPCC. (2013). *Climate Change 2013: The Physical Science Basis. Contribution of Working Group I to the Fifth Assessment Report of the Intergovernmental Panel on Climate Change*. (V. B. and P. M. M. Stocker, T.F., D. Qin, G.-K. Plattner, M. Tignor, S.K. Allen, J. Boschung, A. Nauels, Y. Xia, Ed.), *the Fifth Assessment Report* (Vol. 5). Cambridge and New York: Cambridge University Press.

Kaspari, S., Painter, T. H., Gysel, M., Skiles, S. M., Schwikowski, M. (2014). Seasonal and elevational variations of black carbon and dust in snow and ice in the Solu-Khumbu, Nepal and estimated radiative forcings. *Atmospheric Chemistry and Physics*, *14*(15), 8089–8103. https://doi.org/10.5194/acp-14-8089-2014

Kaspari, S. D., Schwikowski, M., Gysel, M., Flanner, M. G., Kang, S., Hou, S., Mayewski, P. A. (2011). Recent increase in black carbon concentrations from a Mt. Everest ice core spanning 1860-2000 AD. *Geophysical Research Letters*, *38*(4), 11–16.

https://doi.org/10.1029/2010GL046096

Katich, J. M., Perring, A. E., Schwarz, J. P. (2017). Optimized detection of particulates from liquid samples in the aerosol phase: Focus on black carbon. *Aerosol Science and Technology*, *51*(5), 543–553. https://doi.org/10.1080/02786826.2017.1280597

Khan, A. L., McMeeking, G. R., Schwarz, J. P., Xian, P., Welch, K. A., Berry Lyons, W., McKnight, D. M. (2018). Near-Surface Refractory Black Carbon Observations in the Atmosphere and Snow in the McMurdo Dry Valleys, Antarctica, and Potential Impacts of Foehn Winds. *Journal of Geophysical Research: Atmospheres*, *123*(5), 2877–2887. https://doi.org/10.1002/2017JD027696

Kinase, T., Adachi, K., Oshima, N., Goto-Azuma, K., Ogawa-Tsukagawa, Y., Kondo, Y. et al. (2019). Concentrations and Size Distributions of Black Carbon in the Surface Snow of Eastern Antarctica in 2011. *Journal of Geophysical Research: Atmospheres*, 2019JD030737. https://doi.org/10.1029/2019JD030737

Koch, D., Bond, T. C., Streets, D., Unger, N., van der Werf, G. R. (2007). Global impacts of aerosols from particular source regions and sectors. *Journal of Geophysical Research Atmospheres*, *112*(2), 1–24. https://doi.org/10.1029/2005JD007024

Li, F., Ginoux, P. & Ramaswamy, V. (2008). Distribution, transport, and deposition of mineral dust in the Southern Ocean and Antarctica: Contribution of major sources. *Journal of Geophysical Research: Atmospheres*, *113*(10), 1–15. https://doi.org/10.1029/2007JD009190

Lim, S., Faïn, X., Zanatta, M., Cozic, J., Jaffrezo, J.-L., Ginot, P., Laj, P. (2014). Refractory black carbon mass concentrations in snow and ice: method evaluation and inter-comparison with elemental carbon measurement. *Atmospheric Measurement Techniques Discussions*, *7*(4), 3549–3589. https://doi.org/10.5194/amtd-7-3549-2014

Lim, Saehee, Faïn, X., Ginot, P., Mikhalenko, V., Kutuzov, S., Paris, J., Kozacheck, Laj, P. (2017). Black carbon variability since preindustrial times in the eastern part of Europe reconstructed from Mt. Elbrus, Caucasus, ice cores. *Atmospheric Chemistry and Physics*, *17*(5), 3489–3505. https://doi.org/10.5194/acp-17-3489-2017

Mahowald, N., Albani, S., Kok, J. F., Engelstaeder, S., Scanza, R., Ward, D. S., Flanner, M. G. (2014). The size distribution of desert dust aerosols and its impact on the Earth system. *Aeolian Research*, *15*, 53–71. https://doi.org/10.1016/j.aeolia.2013.09.002

Marquetto, L., Kaspari, S., Simões, J. C. (2019). Refractory Black carbon (rBC) variability in a 47-year West Antarctic Snow and Firn core. *Manuscript Submitted for Publication, available at https://www.the-cryosphere-discuss.net/tc-2019-207/#discussion*.

Marquetto, L., Kaspari, S., Simões, J. C., Babik, E. (2020). Refractory Black Carbon results and a method comparison between solid-state cutting and continuous melting sampling of a West Antarctic snow and firn core. *Advances in Atmospheric Sciences*, *37*(February), 1–10.

McConnell, J. R., Edwards, R., Kok, G. L., Flanner, M. G., Zender, C. S., Saltzman, E. S. et al.

(2007). 20th-Century Industrial Black Carbon Emissions Altered Arctic Climate Forcing. *Science*, *317*(September), 1381–1384.

Mori, T., Moteki, N., Ohata, S., Koike, M., Goto-Azuma, K., Miyazaki, Y., Kondo, Y. (2016). Improved technique for measuring the size distribution of black carbon particles in liquid water. *Aerosol Science and Technology*, *50*(3), 242–254. https://doi.org/10.1080/02786826.2016.1147644

Mori, T., Goto-Azuma, K., Kondo, Y., Ogawa-Tsukagawa, Y., Miura, K., Hirabayashi, M. et al. (2019). Black Carbon and Inorganic Aerosols in Arctic Snowpack. *Journal of Geophysical Research: Atmospheres*, 2019JD030623. https://doi.org/10.1029/2019JD030623

Moteki, N., Kondo, Y., Oshima, N., Takegawa, N., Koike, M., Kita, K., Matsui, H., Kajino, M. (2012). Size dependence of wet removal of black carbon aerosols during transport from the boundary layer to the free troposphere. *Geophysical Research Letters*, *39*(13), 2–5. https://doi.org/10.1029/2012GL052034

Moteki, N. & Kondo, Y. (2010). Dependence of laser-induced incandescence on physical properties of black carbon aerosols: Measurements and theoretical interpretation. *Aerosol Science and Technology*, *44*(8), 663–675. https://doi.org/10.1080/02786826.2010.484450

Moteki, N., Kondo, Y., Takegawa, N. Nakamura, S.-ichi. (2009). Directional dependence of thermal emission from nonspherical carbon particles. *Journal of Aerosol Science*, *40*(9), 790–801. https://doi.org/10.1016/j.jaerosci.2009.05.003

Ohata, S., Moteki, N., Schwarz, J. P., Fahey, D. W., Kondo, Y. (2013). Evaluation of a Method to Measure Black Carbon Particles Suspended in Rainwater and Snow Samples. *Aerosol Science and Technology*, *47*(10), 1073–1082. https://doi.org/10.1080/02786826.2013.824067

Osmont, D., Sigl, M., Eichler, A., Jenk, T. M., Schwikowski, M. (2018). A Holocene black carbon ice-core record of biomass burning in the Amazon Basin from Illimani, Bolivia. *Climate of the Past Discussions*, *15*, 579–592. https://doi.org/10.5194/cp-2018-136

Osmont, D., Wendl, I. A., Schmidely, L., Sigl, M., Vega, C. P., Isaksson, E., Schwikowski, M. (2018). An 800 year high-resolution black carbon ice-core record from Lomonosovfonna, Svalbard. *Atmospheric Chemistry and Physics Discussions*, 1–30. https://doi.org/10.5194/acp-2018-244

Pan, X., Kanaya, Y., Taketani, F., Miyakawa, T., Inomata, S., Komazaki, Y. et al. (2017). Emission characteristics of refractory black carbon aerosols from fresh biomass burning: A perspective from laboratory experiments. *Atmospheric Chemistry and Physics*, *17*(21), 13001–13016. https://doi.org/10.5194/acp-17-13001-2017

Petzold, A., Ogren, J. A., Fiebig, M., Laj, P., Li, S. M., Baltensperger, U. et al. (2013). Recommendations for reporting black carbon measurements. *Atmospheric Chemistry and Physics*, *13*(16), 8365–8379. https://doi.org/10.5194/acp-13-8365-2013

635 Reid, J. S., Koppmann, R., Eck, T. F. Eleuterio, D. P. (2005). A review of biomass burning
636 emissions part II: intensive physical properties of biomass burning particles. *Atmospheric*
637 *Chemistry and Physics*, *5*(3), 799–825. https://doi.org/10.5194/acp-5-799-2005

638 Schwanck, F., Simões, J. C., Handley, M., Mayewski, P. A., Bernardo, R. T., Aquino, F. E.
639 (2016). Anomalously high Arsenic concentration in a West Antarctic ice core and its
640 relationship to copper mining in Chile. *Atmospheric Environment*, *125*, 257–264.
641 https://doi.org/dx.doi.org/10.1016/j.atmosenv.2015.11.027

642 Schwanck, F., Simões, J. C., Handley, M., Mayewski, P. A., Auger, J. D., Bernardo, R. T.,
643 Aquino, F. E. (2017). A 125-year record of climate and chemistry variability at the Pine
644 Island Glacier ice divide, Antarctica. *Cryosphere*, *11*(4), 1537–1552.
645 https://doi.org/10.5194/tc-11-1537-2017

646 Schwarz, J. P., Doherty, S. J., Li, F., Ruggiero, S. T., Tanner, C. E., Perring, A. E., Gao, R. S.,
647 Fahey, D. W. (2012). Assessing Single Particle Soot Photometer and Integrating
648 Sphere/Integrating Sandwich Spectrophotometer measurement techniques for quantifying
649 black carbon concentration in snow. *Atmospheric Measurement Techniques*, *5*(11), 2581–
650 2592. https://doi.org/10.5194/amt-5-2581-2012

651 Schwarz, J P, Spackman, J. R., Gao, R. S., Perring, A. E., Cross, E., Onasch, T. B. et al. (2010).
652 The Detection Efficiency of the Single Particle Soot Photometer. *Aerosol Science and*
653 *Technology*, *44*(8), 612–628. https://doi.org/10.1080/02786826.2010.481298

654 Schwarz, J P, Gao, R. S., Perring, a E., Spackman, J. R., Fahey, D. W. (2013). Black carbon
655 aerosol size in snow. *Nature Scientific Reports*, *3*, 1356. https://doi.org/10.1038/srep01356

656 Schwarz, Joshua P., Gao, R. S., Fahey, D. W., Thomson, D. S., Watts, L. A., Wilson, J. C. et al.
657 (2006). Single-particle measurements of midlatitude black carbon and light-scattering
658 aerosols from the boundary layer to the lower stratosphere. *Journal of Geophysical*
659 *Research Atmospheres*, *111*(16), 1–15. https://doi.org/10.1029/2006JD007076

660 Sigl, M., Abram, N. J., Gabrieli, J., Jenk, T. M., Osmont, D., Schwikowski, M. (2018). 19th
661 century glacier retreat in the Alps preceded the emergence of industrial black carbon
662 deposition on high-alpine glaciers. *The Cryosphere*, *12*(10), 3311–3331.
663 https://doi.org/10.5194/tc-12-3311-2018

664 Sinha, P. R., Kondo, Y., Goto-Azuma, K., Tsukagawa, Y., Fukuda, K., Koike, M. et al. (2018).
665 Seasonal Progression of the Deposition of Black Carbon by Snowfall at Ny-Ålesund,
666 Spitsbergen. *Journal of Geophysical Research: Atmospheres*, *123*(2), 997–1016.
667 https://doi.org/10.1002/2017JD028027

668 Slowik, J. G., Cross, E. S., Han, J.-H., Davidovits, P., Onasch, T. B., Jayne, J. T. et al. (2007).
669 An Inter-Comparison of Instruments Measuring Black Carbon Content of Soot Particles.
670 *Aerosol Science and Technology*, *41*(3), 295–314.
671 https://doi.org/10.1080/02786820701197078

672 Stohl, A. & Sodemann, H. (2010). Characteristics of atmospheric transport into the Antarctic

673 troposphere. *Journal of Geophysical Research: Atmospheres*, *115*(D2), 1–16.
674 https://doi.org/10.1029/2009JD012536

675 Symonds, J. P. R., Reavell, K. S. J., Olfert, J. S. (2013). The CPMA-electrometer system - A
676 suspended particle mass concentration standard. *Aerosol Science and Technology*, *47*(8).
677 https://doi.org/10.1080/02786826.2013.801547

678 Technologies, D. M. (2013a). PSI Toolkit for the Single Particle Soot Manual - DOC-0359
679 Revision A. Boulder, CO: Droplet Measurement Technologies.

680 Technologies, D. M. (2013b). Single Particle Soot Photometer (SP2) Operator Manual.

681 Thevenon, F., Anselmetti, F. S., Bernasconi, S. M., Schwikowski, M. (2009). Mineral dust and
682 elemental black carbon records from an Alpine ice core (Colle Gnifetti glacier) over the last
683 millennium. *Journal of Geophysical Research Atmospheres*, *114*(17), 1–11.
684 https://doi.org/10.1029/2008JD011490

685 Wang, Q., Schwarz, J. P., Cao, J., Gao, R., Fahey, D. W., Hu, T., Huang, R.-J., Han, Y., Shen, Z.
686 (2014). Black carbon aerosol characterization in a remote area of Qinghai-Tibetan plateau,
687 western China. *Science of the Total Environment*, *479–480*(1), 151–158.
688 https://doi.org/10.1016/j.scitotenv.2014.01.098

689 Wang, Q. Y., Huang, R. J., Cao, J. J., Tie, X. X., Ni, H. Y., Zhou, Y. Q. et al. (2015). Black
690 carbon aerosol in winter northeastern Qinghai-Tibetan Plateau, China: The source, mixing
691 state and optical property. *Atmospheric Chemistry and Physics*, *15*(22), 13059–13069.
692 https://doi.org/10.5194/acp-15-13059-2015

693 Warren, S. G. & Wiscombe, W. J. (1980). A Model for Spectral Albedo of Snow II: Snow
694 containing Atmospheric Aerosols. *Journal of the Atmospheric Sciences*, *37*, 2734–2745.

695 Wendl, I. a., Menking, J. A., Färber, R., Gysel, M., Kaspari, S. D., Laborde, M. J. G.,
696 Schwikowski, M. (2014). Optimized method for black carbon analysis in ice and snow
697 using the Single Particle Soot Photometer. *Atmospheric Measurement Techniques*
698 *Discussions*, *7*(3), 3075–3111. https://doi.org/10.5194/amtd-7-3075-2014

699 Wu, Y., Wang, X., Tao, J., Huang, R., Tian, P., Cao, J. et al. (2017). Size distribution and source
700 of black carbon aerosol in urban Beijing during winter haze episodes. *Atmospheric*
701 *Chemistry and Physics*, *17*(12), 7965–7975. https://doi.org/10.5194/acp-17-7965-2017

702

703
704